Uncovering spectral repulsion in extended quasienergy states

W. A. Lin and L. E. Reichl
Ilya Prigogine Center for Statistical Mechanics, University of Texas, Austin, Texas 78712
(Received 3 February 1989)

We study classical and quantum mechanics of a rotor in the presence of two interacting nonlinear resonances. Quasienergy states and quasienergies are computed. The widths of the quasienergy states in the representation of the unperturbed angular-momentum levels are found to be closely associated with the classical dynamics. The widths of many resonant quasienergy states are found to be extended by the quantum-resonance overlap when the perturbation is increased. Spectral repulsion is present in these extended states.

I. INTRODUCTION

The ubiquity of chaos in classical nonintegrable systems has tempted many researchers to look for its quantum counterpart. While no sensitive dependence on initial conditions has been obtained, there exist similarities between classical and quantum dynamics. At the classical level, it has been well established[1] that, for near-integrable Hamiltonian systems with two degrees of freedom, transition to global chaos occurs in regions of phase space where primary resonance zones overlap. Such a transition is signified by a sudden increase in the region of phase space that can be explored by the trajectories at the chaotic separatrix layers of the primary resonances as the sizes of the resonance zones are increased. The quantum manifestation of this phenomenon[2,3] is a sudden increase in the region of Hilbert space that can be effectively explored by the wave function due to overlap of quantum-resonance zones.

Classically, resonance overlap leads to the destruction of Kolmogorov-Arnold-Moser (KAM) tori, which is equivalent to the destruction of a local constant of the motion. We have shown[4] that the quantum manifestation of such a phenomenon appears to be the destruction of a local quantum number through quantum-resonance overlap, accompanied by the emergence of the spectral repulsion[4,5] as well as the long-range spectral rigidity.[4]

Quantum-resonance overlap and the consequent spreading of the wave function suggest that the widths of quasienergy states (for the case of a time periodic Hamiltonian) in a proper representation will be extended by the overlap.[6] The destruction of a local quantum number, which appears to accompany quantum-resonance overlap, then suggests that spectral repulsion and rigidity might be associated with these extended states. The aim of this paper is to demonstrate these two points.

We begin in Sec. II with a description of the model and computation of classical trajectories in phase space. In Sec. III, we compute the quasienergy states and quasienergies of the corresponding quantum system and compare them with the classical phase-space structure. In Sec. IV the quasienergy states are divided into different classes. The spectral statistics for each class is then computed. In Sec. V we make some concluding remarks.

II. CLASSICAL TRAJECTORIES

We consider the Hamiltonian of a free rotor in the presence of two interacting nonlinear resonances,[7]

$$H=\frac{J^2}{2mr^2}+\lambda\cos(\phi-\omega_0 t)+\lambda\cos(3\phi-\omega_0 t)\ , \tag{2.1}$$

where J is the angular momentum, ϕ is the angle of rotation, m is the mass, r is the radius of rotation, λ and ω_0 are the amplitude and angular frequency of the rotating waves, respectively, and t is the time. Let us define $\Omega\equiv\hbar/2mr^2$. For convenience, we make a canonical transformation, with the new Hamiltonian $H'=H/\hbar\Omega$, the new canonical momentum $I=J/\hbar$, and the new time $t'=\Omega t$, together with $\omega'\equiv\omega_0/\Omega$ and $Q\equiv\lambda/2\hbar\Omega$,

$$H'=I^2+2Q\cos(\phi-\omega' t')+2Q\cos(3\phi-\omega' t')\ . \tag{2.2}$$

All quantities are now dimensionless.

Each cosine wave in Eq. (2.2) gives rise to a primary resonance zone. For Q small enough, the two zones will be well separated and we can use a single-resonance approximation to describe the location and width of each of the two zones. The first cosine wave gives rise to a period-one primary resonance zone centered at $I=\omega'/2$ with width $4\sqrt{Q}$, and the second cosine wave gives rise to a period-three primary resonance zone centered at $I=\omega'/6$ with width $4\sqrt{Q}$. Throughout our computations, we have chosen $\omega'=120$. Thus by the overlap criterion,[8] the two zones overlap at $Q=100$.

In Fig. 1 we have plotted numerically computed trajectories in the phase plane (ϕ,I) for the Poincaré surface of section computed at times $t'=n\tau'$, where n is an integer and τ' $(=2\pi/\omega')$ is the period of the waves. We give our results for a range of different Q's. At $Q=50$, the existence of KAM tori between the two primary resonance zones is evident. The transition to global chaos occurs between $Q=80$ and 90. For larger values of Q, we see a diminishing in the size of the period-one stable island with increasing Q. At $Q=800$, it is totally wiped out. On the other hand, the period-three stable islands behave quite differently. These are never totally destroyed and are smallest at $Q=400$. $Q=400$ is the value of Q at which the separatrix of one resonance zone touches the

center of the other when using the single-resonance approximation. Beyond that we see the growth of the stable islands but with fluctuations such as the one at $Q=800$. A further increase in Q to 1600 does not help to reduce the sizes of the stable islands. For the nonresonant trajectories, the closer they are to the resonance zones, the larger the variations in action.

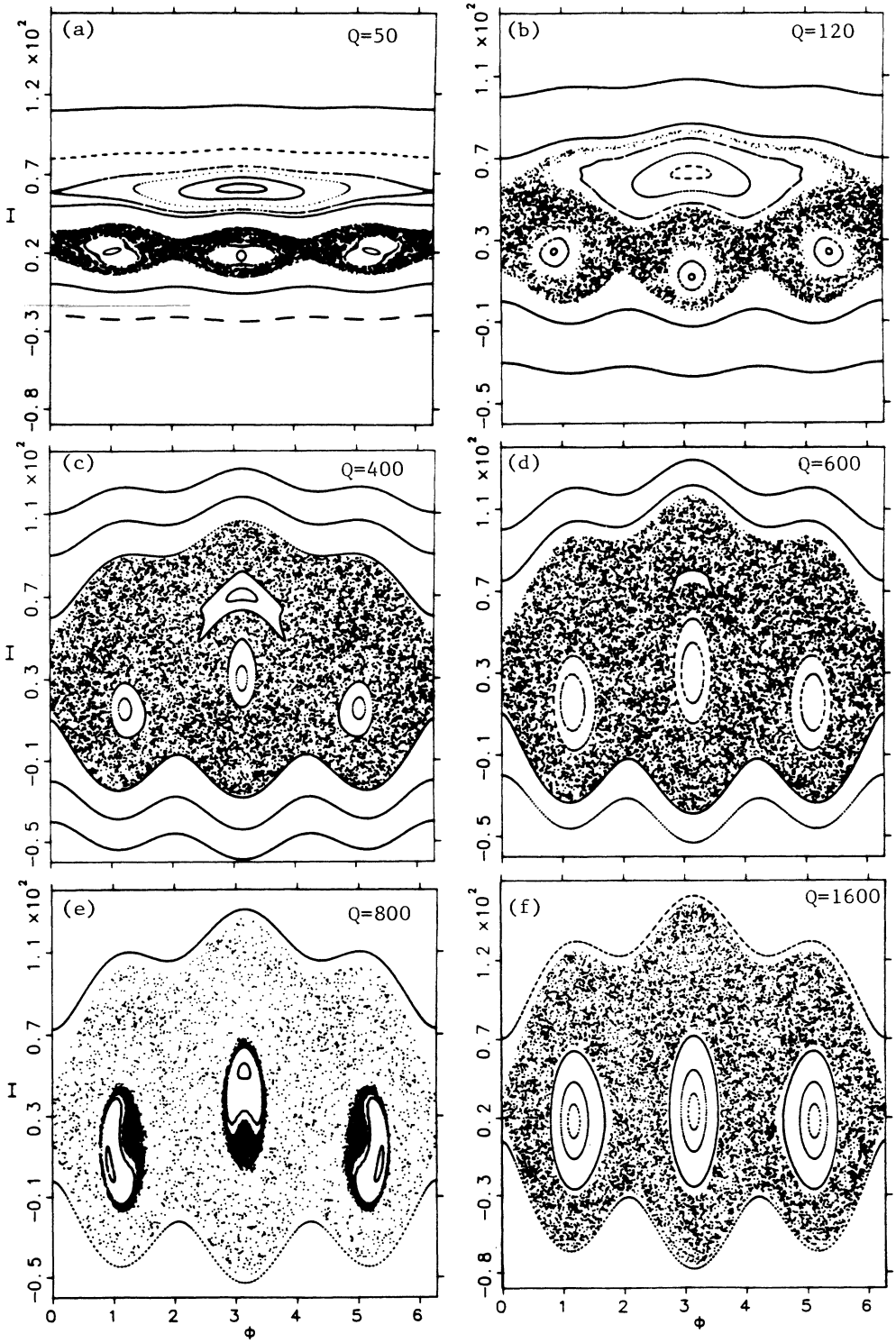

FIG. 1. Trajectories of Eq. (2.2) at Poincaré sections. (a) $Q=50$; (b) $Q=120$; (c) $Q=400$; (d) $Q=600$; (e) $Q=800$, the blackened chaotic areas and the rest of the chaotic sea is a single trajectory; (f) $Q=1600$.

III. QUASIENERGY STATES

The Schrödinger equation for this system takes the following form:

$$i\frac{\partial|\psi(t')\rangle}{\partial t'}=[\hat{I}^2+2Q\cos(\hat{\phi}-\omega' t')+2Q\cos(3\hat{\phi}-\omega' t')]|\psi(t')\rangle\ . \tag{3.1}$$

Due to the periodicity of the Hamiltonian, the general solution of the above equation can be written as a linear combination of quasienergy states, $|\psi_{\mathcal{E}_i}(t')\rangle=|u_{\mathcal{E}_i}(t')\rangle e^{-i\mathcal{E}_i t'}$, where $|u_{\mathcal{E}_i}(t')\rangle=|u_{\mathcal{E}_i}(t'+\tau')\rangle$, and $\mathcal{E}_i(\mathrm{mod}\omega')$ is the quasienergy.[9,10] Let us denote $\hat{T}(t')$ as the time development operator,

$$|\psi(t')\rangle=\hat{T}(t')|\psi(0)\rangle\ . \tag{3.2}$$

Then we have[10]

$$\hat{T}(\tau')|\psi_{\mathcal{E}_i}(0)\rangle=e^{-i\mathcal{E}_i\tau'}|\psi_{\mathcal{E}_i}(0)\rangle\ . \tag{3.3}$$

Let us work in the representation consisting of eigenstates of $\hat{I}$, $|j\rangle$ ($\hat{I}|j\rangle=j|j\rangle$, j is an integer). In this representation, the Schrödinger equation takes the form

$$i\frac{\partial\langle j|\psi(t')\rangle}{\partial t'}=j^2\langle j|\psi(t')\rangle+Q\sum_{N=1,3}[e^{-i\omega' t'}\langle j-N|\psi(t')\rangle+e^{i\omega' t'}\langle j+N|\psi(t')\rangle]\ . \tag{3.4}$$

Matrix elements $\langle j|\hat{T}(\tau')|k\rangle$ can be obtained from Eq. (3.4) if we note that $\langle j|\psi(\tau')\rangle=\sum_k\langle j|\hat{T}(\tau')|k\rangle\langle k|\psi(0)\rangle$. If we now choose $\langle k|\psi(0)\rangle=\delta_{kj'}$, then we obtain $\langle j|\psi(\tau')\rangle=\langle j|\hat{T}(\tau')|j'\rangle$. Therefore $\langle j|\psi(\tau')\rangle$ is obtained by numerically integrating Eq. (3.4) with such initial conditions, from which we obtain the matrix elements of $\hat{T}(\tau')$. We can then compute the eigenvalues and eigenvectors of this matrix numerically. These eigenvectors are the quasienergy states $|\psi_{\mathcal{E}_i}(0)\rangle$ of the system. We found that for this system $\langle j|\psi_{\mathcal{E}_i}(0)\rangle$ have finite extent. And therefore it is possible to truncate the Hilbert space and obtain accurate results. The quasienergy states thus obtained are only those which will contribute significantly to the chosen part of Hilbert space. For our purpose, the levels used cover the two quantum-resonance zones, the region in between, as well as parts of the adjacent nonresonant regions.

Figure 2 shows some of the $|\langle j|\psi_{\mathcal{E}_i}(0)\rangle|^2$ terms so obtained. From the many graphs of quasienergy states that we obtained, we noticed the following general characteristic. We can clearly distinguish the locations of the resonance zones and the nonresonant regions. In the resonance zones, there are wider quasienergy states that are much more perturbed away from the unperturbed eigenstates as compared with those residing in the nonresonant regions. In the nonresonant regions, the wider a quasienergy state is, the closer it gets to the resonance zone. This corresponds to a larger variation in I for a nonresonant classical trajectory as it gets closer to a resonant zone. In a resonance zone, the widths of quasienergy states vary from the most localized state with its peak located nearly at the corresponding classical elliptic fixed point, to wider states with their widths corresponding to the variations in I of the corresponding classical trajectories in the stable resonance islands, to widest states corresponding to the classical chaotic trajectories along the separatrix layers.

For example, at $Q=50$ [Fig. 2(a)], the most localized state in the period-one zone is peaked at near $j=60$, and the most localized state in the period-three zone is peaked at near $j=20$ [cf. Fig. 2(a), part (IV)]. It is evident that, from the corresponding classical figure [Fig. 1(a)], these are the locations of the elliptic fixed points. A comparison of Figs. 1(a) and 2(a) part (V) and 2(a) part (VI) shows that the widest state in period-one zone spans a region approximately equal to the corresponding classical resonance zone and similarly for the widest state in period-three zone. Obviously, the two zones have not overlapped yet. Indeed, Fig. 2(a) part (III) shows one of the widest states located in the nonresonant region between the two zones. The presence of localized states in this region is a quantum manifestation of the existence of KAM tori.[11,4]

Similar to the classical dynamics, the overlap of the two zones appears to occur also near $Q=90$, where there is a state with its appreciable amplitudes covering the entire period-three zone and extends beyond $j=60$. At $Q=100$, the overlap definitely has occurred, where there is a state covering the two overlapped resonance zones. At $Q=120$ [Fig. 2(b)], there are about ten fully extended states covering the entire region of overlapped zones. One of them is shown in Fig. 2(b) part (III).

At $Q=400$ [Fig. 2(c)], for the states in the overlapped zones, there is only one localized state. It is confined in a region corresponding to the classical period-one stable island, as seen in the right state in Fig. 2(c) part (II). There are also three localized states confined in a region corresponding to the classical period-three stable islands. One of them is seen as the left one of Fig. 2(c) part (II). For the rest of the resonant states, a total of 103, most of them are fully extended states covering a region approximately equal to that of the corresponding classical chaotic trajectories. Only a few are less extended but still with appreciable amplitudes going beyond the borders of the classical stable islands $I\simeq 0$ and 85.

At $Q=600$ [Fig. 2(d)], there is no localized state which can be associated with the classical period-one stable island. The number of localized states which are basically confined within the boundaries of classical period-three stable islands, $I\simeq -10$ to 61, is 11. The remaining of the resonant states, a total of 106, are mostly fully extended.

At $Q=800$ [Fig. 2(e)], similarly, we do not find any localized state that can be associated with the corresponding classical period-one stable island. But there are about 16 period-three localized states with appreciable amplitudes confined within the interval $[-18,69]$. It appears that these cannot all be associated with the classical stable islands, since the total phase-space area is smaller than the case with $Q=600$. But Fig. 1(e) suggests the presence of cantori,[12,13] separating the blackened part of

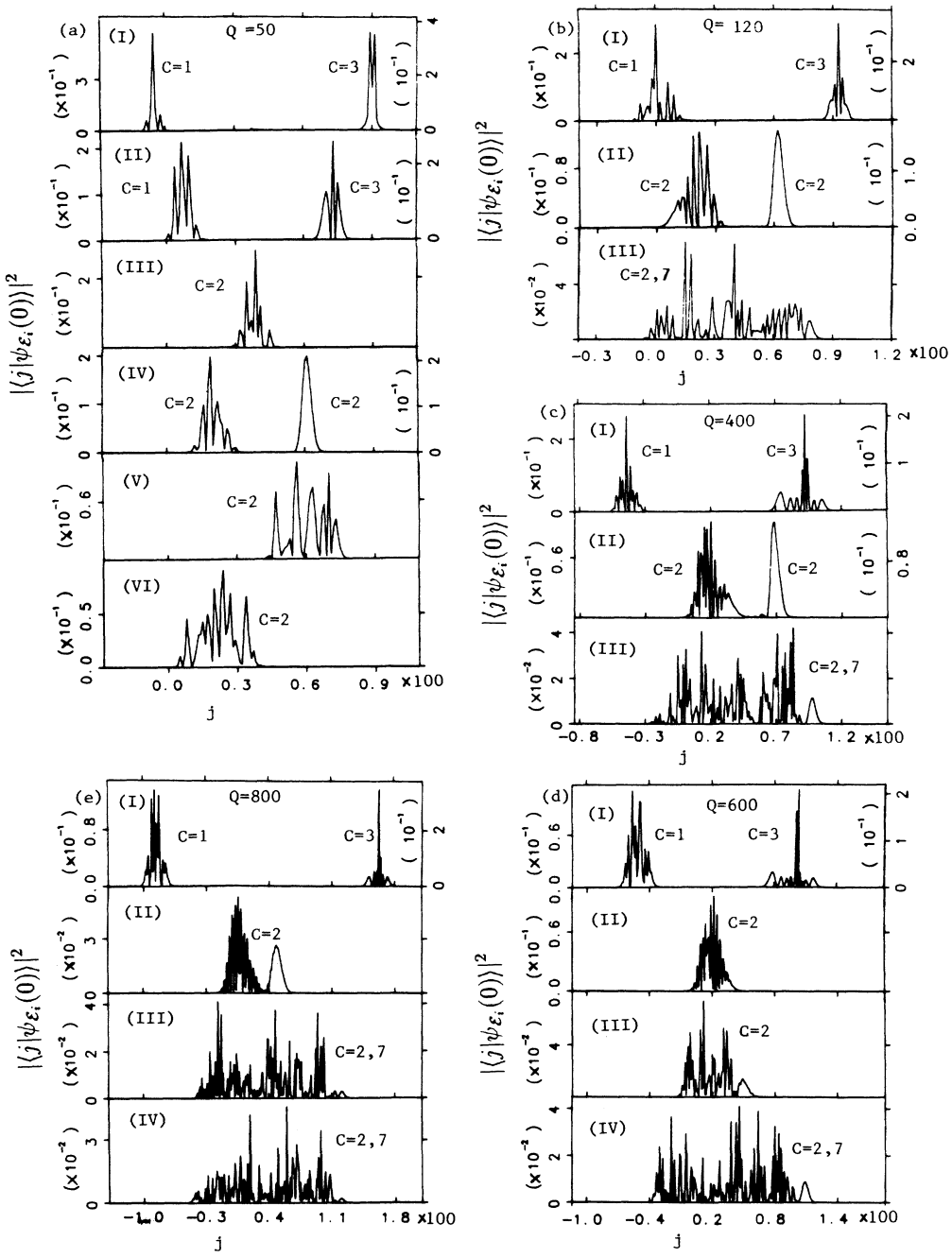

FIG. 2. Selected quasienergy states. Each quasienergy state is labeled according to the class of spectrum to which it belongs. In addition to the ones explicitly shown, all states also belong to the $C=6$ class. $C=1$ and 3 states also belong to the $C=4$ class. So, for $C=1$, it also means $C=1,4,6$. For $C=3$, it also means $C=3,4,6$. For $C=2$, it also means $C=2,6$. For $C=2,7$, it also means $C=2,7,6$. Note that in some cases we have included two different eigenstates on a single plot [for example, (a) parts (I), (II), and (IV)]. (a) $Q=50$; (I) and (II): states in the nonresonant regions; (III): a state in the nonresonant region between the two resonance zones; (IV): the most localized states in the period-one zone (right) and the period-three zone (left); (V): the widest state in period-one zone; (VI): the widest state in period-three zone. (b) $Q=120$; (I): nonresonant states; (II): the most localized states in the two resonance zones; (III): a fully extended state. (c) $Q=400$; (I): nonresonant states; (II): the most localized states in the two resonance zones; (III): a fully extended state. (d) $Q=600$; (I) nonresonant states; (II) and (III): localized states in the period-three zone; (IV): a fully extended state. (e) $Q=800$; (I): nonresonant states; (II): the most localized state in the period-three zones; (III) and (IV): fully extended states.

the trajectory and the rest of the trajectory in the chaotic sea. The trajectory initially starts at (3.1416, 20) in the blackened area and it took a long time to escape into the big chaotic sea. It has been shown,[14–17] that cantori have the effect of inhibiting the propagation of probability amplitudes. The area bounded by the cantori is bigger than the area of the period-three stable islands at $Q=600$. Consequently, it is able to support more localized states. An example of the localized states is shown in Fig. 2(e) part (II). It is peaked around $j\simeq 6$ and 47, which are very close to the corresponding classical period-three fixed points. Thus it is easy to convince ourselves that such a state is associated with the classical period-three stable island. Again, the rest of the resonant states, a total of 114, are mostly fully extended [Fig. 2(e) parts (III) and (IV)].

From the above, we can clearly see that the extended states emerge as the two quantum-resonance zones overlap. A comparison of Figs. 1 and 2 shows that the widths and locations of the fully extended states are closely given by the corresponding classical chaotic trajectories.

IV. SPECTRAL STATISTICS OF THE QUASIENERGY STATES

We first compute the distribution of nearest-neighbor spacings of the quasienergy energy levels.[18,4] As we have explained in Sec. III, we know the locations and widths of the resonance zones, therefore we can divide the states into classes for the purpose of analyzing their spectrum. For each Q, the quasienergy states are divided into the following classes.

(a) $C=1$ denotes those states located in the nonresonant lower-j side of period-three resonance zone.

(b) $C=3$ denotes those states located in the nonresonant higher-j side of period-one resonance zone.

(c) $C=2$ denotes any state located in between $C=1$ and 3 nonresonant regions. In addition to these, we also define three other classes.

(d) $C=4$ denotes all states in $C=1$ and 3.

(e) $C=6$ denotes all states in $C=1$, 2, and 3.

(f) $C=7$ denotes all states in $C=2$ but excluding the localized states in that class. The $C=7$ states are the extended states. From these definitions, we see that the set of $C=7$ states is a subset of the set of $C=2$ states, which in turn is a subset of the set of $C=6$ states. When selecting $C=1$ and 3 states for computing statistics, we have eliminated those states affected by our truncation of the Hilbert space, that is, those which are too close to the edges of the truncated region.

To improve statistics,[19] we use the spectra from four nearby Q's to compute the spacing distribution. We have computed the statistics for five sets of Q's: (1) $Q=20$, 30,40,50; (2) $Q=90,100,110,120$; (3) $Q=370,380,390,400$; (4) $Q=570,580,590,600$; (5) $Q=770,780,790,800$. For each Q in a given set, we pick out the spectrum for a given class. This is then multiplied by a factor so that the resulting spectra from the four Q's have the same mean spacing. This is the only unfolding[18] we have done. In our previous work,[4] we have used a different method to obtain the quasienergy spectrum. The spectrum was obtained by a Fourier analysis of a state initially occupying only a single unperturbed level in a proper part of Hilbert space. As a result of the Fourier analysis, the spectrum obtained covered many intervals of the angular frequency of the external field times $\hbar$. Therefore a proper unfolding was necessary.

To measure the amount of spectral repulsion, a nonlinear least-squares method is used to fit the computed distribution with the Brody distribution,[20]

$$P_q(x)=(1+q)B(q)x^q\exp[-B(q)x^{1+q}]\,, \tag{4.1}$$

where $B(q)=[\Gamma((2+q)/(1+q))]^{1+q}$, x is the spacing in units of local average spacing, and q is the Brody parame-

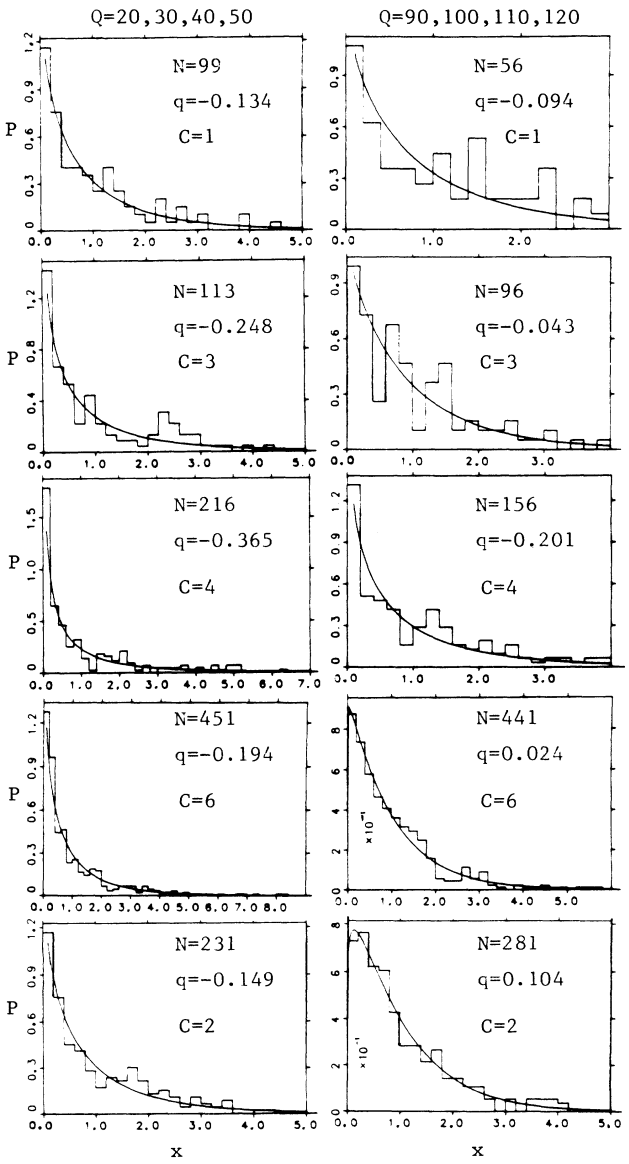

FIG. 3. Distribution of the nearest-neighbor spacings for each class of quasienergy spectrum. In this figure and Fig. 4, N is the number of spacings and q is the Brody parameter. (Column 1): $Q=20,30,40,50$; (column 2): $Q=90,100,110,120$.

ter. When $q<0$ there is spectral attraction and when $q>0$ there is spectral repulsion.

Our results for the spacing distributions are shown in Figs. 3 and 4. From these figures, we can see clearly that the spectral repulsion emerges when quantum-resonance zones overlap and it is dominantly associated with the extended states. Such repulsion is made much more visible by isolating the cause. Otherwise, as in the case of $C=6$

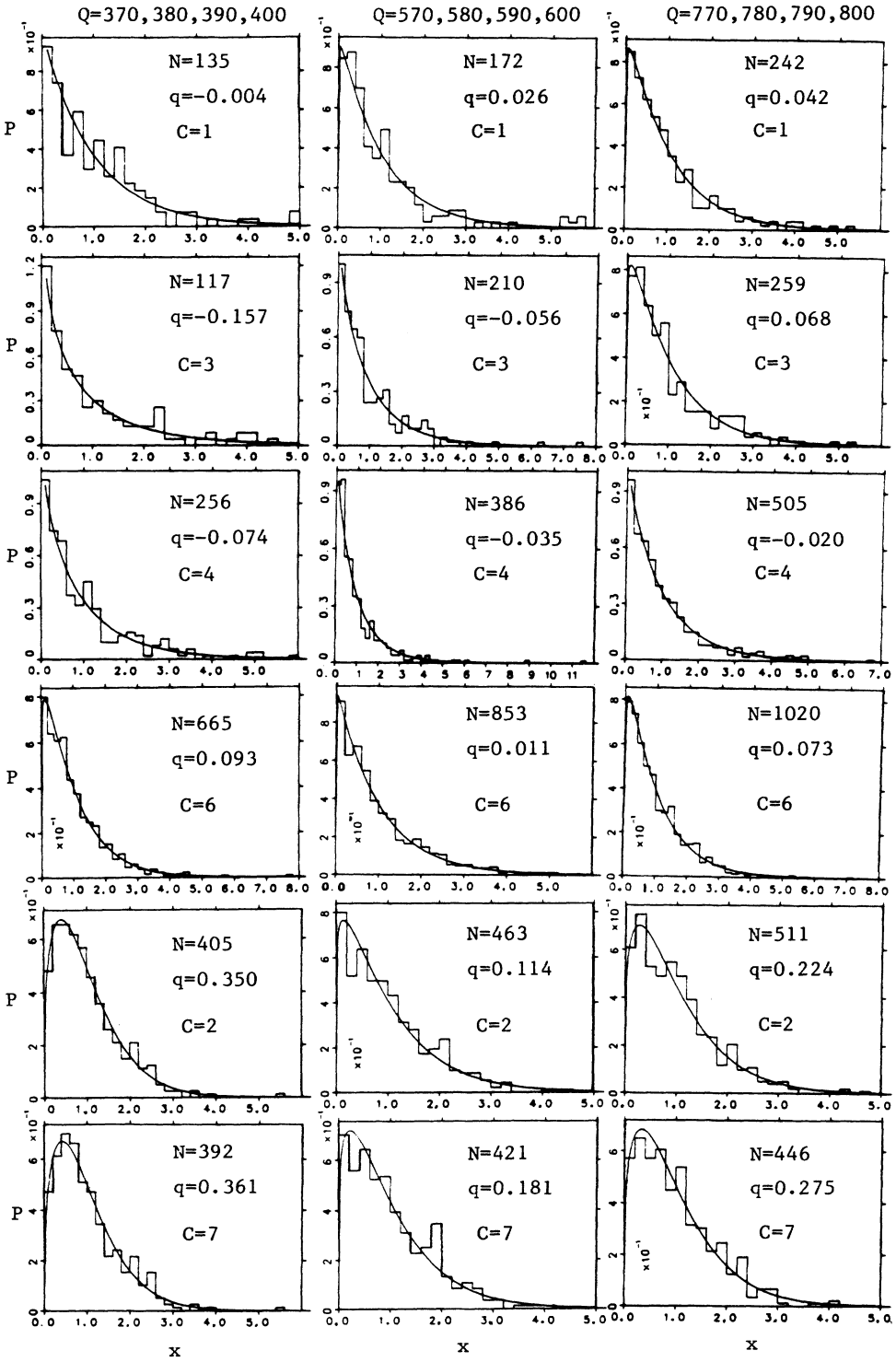

FIG. 4. Distribution of the nearest-neighbor spacings for each class of quasienergy spectrum. (Column 1): $Q=370,380,390,400$; (column 2): $Q=570,580,590,600$; (columns 3): $Q=770,780,790,800$.

spectra, it is immersed in the $C=4$ spectra and harder to see.

We next compute the Δ_3 statistics of Dyson and Mehta,[21]

$$\Delta_3(n,\mathcal{E}')=\frac{1}{n\bar{D}}\min_{A_1,A_2}\int_{\mathcal{E}'}^{\mathcal{E}'+n\bar{D}}[F(\mathcal{E})-A_1\mathcal{E}-A_2]^2 d\mathcal{E}\ . \tag{4.2}$$

The interval $[\mathcal{E}',\mathcal{E}+n\bar{D}]$ contains n spacings, $\bar{D}$ is the average spacing over the interval, and $F(\mathcal{E})$ is the staircase function of an unfolded spectrum. A_1 and A_2 are chosen to minimize the integral. For each Q, a spectral averaged Δ_3 statistic[4] is computed for a given class of spectrum. An average from the four nearby Q's is computed. The result is shown in Fig. 5. Our results are consistent with those for the spacing distribution (short-range spectral property). The long-range rigidity is increased by the presence of extended states.

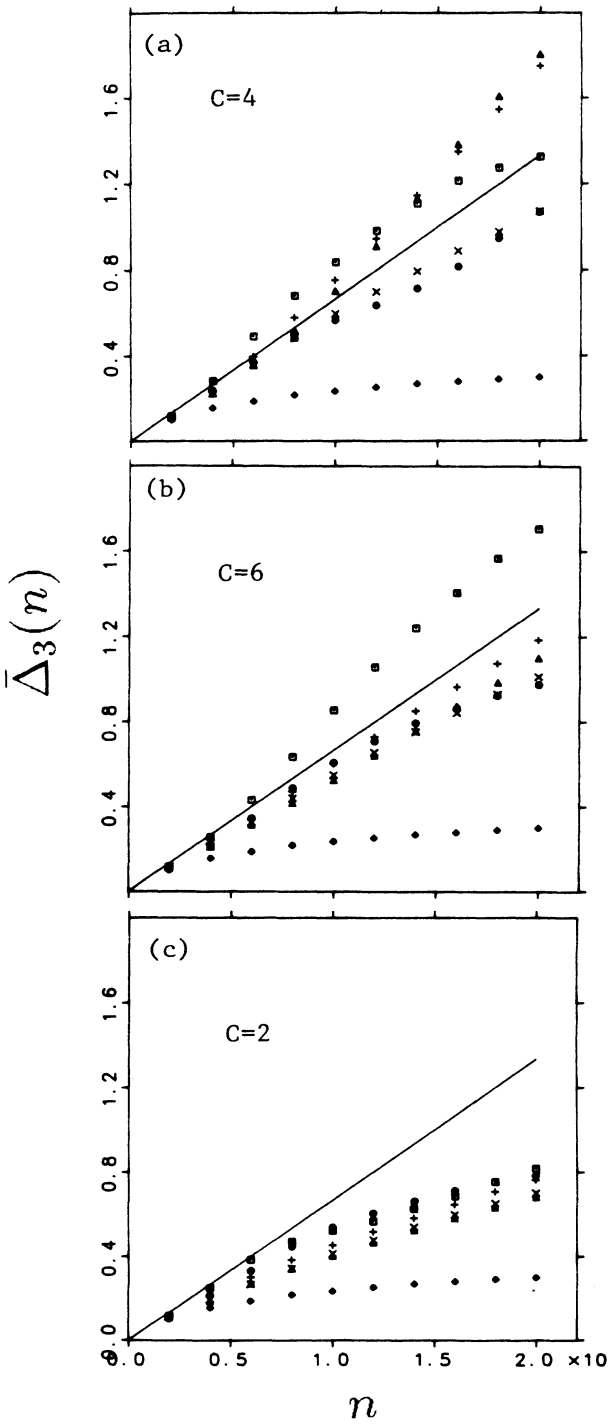

FIG. 5. Spectral averaged Δ_3 statistic; squares: $Q=20,30,40,50$; circles $Q=90,100,110,120$; triangles: $Q=370,380,390,400$; pulses: $Q=570,580,590,600$; $\times$s: $Q=770,780,790,800$; diamonds: GOE; line: $n/15$. (a) $C=4$; (b) $C=6$; (c) $C=2$.

V. DISCUSSIONS AND CONCLUSION

The computations of quantum dynamics shows an extreme similarity with the corresponding classical dynamics and presents further evidence for a "quantum nonlinear dynamics."[22] There are nonresonant localized states corresponding to the classical nonresonant trajectories. There are wider resonant as well as narrower resonant states in the resonance zones similar to the trajectories in the classical resonance zones. At larger Q's, we see the destruction of period-one localized states and the persistence of period-three localized states, And there are extended states,[23] which are the classical analog of chaotic trajectories wandering throughout the region covered by the overlapped resonance zones. They emerge as the quantum-resonance zones overlap. Associated with these extended states is the presence of spectral repulsion. These are the ones which appear to have lost a quantum number.

The degree of spectral repulsion that we obtained, however, is small compared with Gaussian orthogonal ensemble (GOE) results for which $q\simeq 1$. There could be two possible reasons for this. One is the inclusion of some not quite fully extended states in the $C=7$ spectrum. The other reason is that the regime we are in is fully quantal. There has been a great deal of work in which a large degree of spectral repulsion ($q\simeq 1$) was obtained either in the semiclassical regime or when highly excited levels are involved.[24,18] Our results suggest that there might be deviations from GOE in the fully quantal regime. The work of Berman *et al.*[7] also shows a small amount of spectral repulsion. Further work is required to resolve these matters.

The computations of classical dynamics reveals the following questions. Why does the period-one island get destroyed while the period-three islands persist when Q is increased? Is there a point, when Q is increased, beyond which the period-three islands are also totally destroyed? Although considerable efforts have been put into predicting the border of transition to global chaos, relatively less work has been done in understanding the regime beyond the transition. Without understanding this regime our knowledge about resonance overlap will not be complete.

ACKNOWLEDGMENTS

The authors wish to thank the Welch Foundation of Texas for partial support, in particular, Grant No. F-1051. One of us (W.A.L.) would like to thank Professor Peter Koch, Professor M. K. Ali, and Professor Hilda A. Cerdeira for useful conversations. The computations for this work were performed with a Cray X-MP/24 at the University of Texas System Center for High Performance Computing.

[1]A. J. Lichtenberg and M. A. Lieberman, *Regular and Stochastic Motion* (Springer-Verlag, New York, 1983).

[2]G. P. Berman and G. M. Zaslavskii, Phys. Lett. **61A**, 295 (1977); G. P. Berman, G. M. Zaslavskii, and A. R. Kolovsky, *ibid.* **87A**, 152 (1982); G. P. Berman and A. R. Kolovsky, *ibid.* **95A**, 15 (1983); G. P. Berman, G. M. Zaslavskii, and A. R Kolovsky, Zh. Eksp. Teor. Fiz. **81**, 506 (1981) [Sov. Phys.—JETP **54**, 272 (1981)].

[3]L. E. Reichl and W. A. Lin, Phys. Rev. A **33**, 3598 (1986).

[4]W. A. Lin and L. E. Reichl, Phys. Rev. A **36**, 5099 (1987); **37**, 3972 (1988), and references therein; W. A. Lin, Ph.D. dissertation, University of Texas at Austin, 1986, University Microfilms No. 87-06063.

[5]S. Graffi, T. Paul and H. J. Silverstone, Phys. Rev. Lett. **59**, 255 (1987).

[6]For the transition from localized to delocalized quasienergy states see J. N. Bardsley and B. Sundaram, Phys. Rev. A **32**, 689 (1985); J. N. Bardsley, B. Sundaram, L. A. Pinnaduwage, and J. E. Bayfield, Phys. Rev. Lett. **56**, 1007 (1986).

[7]A similar model is considered in G. P. Berman, F. M. Izrailev, and O. F. Vlasova, Zh. Eksp. Teor. Fiz. **93**, 470 (1987) [Sov. Phys.—JETP **66**, 269 (1988)].

[8]B. V. Chirikov, Phys. Rep. **52**, 263 (1979).

[9]Ya. B. Zel'dovich, Zh. Eksp. Teor. Fiz. **51**, 1492 (1966) [Sov. Phys.—JETP **24**, 1006 (1967)]; Ya. B. Zel'dovich, Usp. Fiz. Nauk **110**, 139 (1973) [Sov. Phys.—Usp. **16**, 427 (1973)].

[10]H. Sambe, Phys. Rev. A **7**, 2203 (1973).

[11]G. Hose and H. S. Taylor, Phys. Rev. Lett. **51**, 947 (1983); L. E. Reichl and W. A. Lin, Found. Phys. **17**, 689 (1987).

[12]R. S. Mackay, J. D. Meiss, and I. C. Percival, Physica D **13**, 55 (1984).

[13]D. Bensimon and L. P. Kadanoff, Physica D **13**, 82 (1984).

[14]R. C. Brown and R. E. Wyatt, Phys. Rev. Lett. **57**, 1 (1986).

[15]T. Geisel, G. Radons, and J. Rubner, Phys. Rev. Lett. **57**, 2883 (1986).

[16]E. J. Heller, Phys. Rev. A **35**, 1360 (1987).

[17]R. S. Mackay and J. D. Meiss, Phys. Rev. A **37**, 4702 (1988).

[18]T. A. Brody, J. Flores, J. B. French, P. A. Mello, A. Pandey, and S. S. M. Wong, Rev. Mod. Phys. **53**, 385 (1981).

[19]O. Bohigas, M. J. Giannoni, and C. Schmit, Phys. Rev. Lett. **52**, 1 (1984).

[20]T. A. Brody, Lett. Nuovo Cimento **7**, 482 (1973). See Ref. 4 for the reasons we use this distribution.

[21]F. J. Dyson and M. L. Mehta, J. Math. Phys. **4**, 701 (1963).

[22]J. E. Bayfield, in *Quantum Measurement and Chaos,* edited by E. R. Pike and S. Sarkar (Plenum, New York, 1987).

[23]See also L. E. Reichl, Phys. Rev. A **39**, 4817 (1989); in *Singular Behavior and Nonlinear Dynamics,* edited by St. Pnevmatikos (World Scientific, Singapore, 1989).

[24]M. V. Berry, in *Chaotic Behavior of Deterministic Systems,* Proceedings of the Les Houches Summer School of Theoretical Physics, 1981, edited by G. Iooss, R. H. G. Helleman and R. Stora (North-Holland, Amsterdam, 1983); P. Pechukas, Phys. Rev. Lett. **51**, 943 (1983); Berry and Robnik, J. Phys. A **17**, 2413 (1984); T. H. Seligman, J. J. M. Verbaarschot, and M. R. Zirnbauer, Phys. Rev. Lett. **53**, 215 (1984); T. Terasaka and T. Matsushita, Phys. Rev. A **32**, 538 (1985); J. V. José and R. Cordery, Phys. Rev. Lett. **56**, 290 (1986).